Impact of doping on the ionic conductivity of ceria: A comprehensive model

Hao Wang, Alexander Chroneos, and Udo Schwingenschlögl

Citation: The Journal of Chemical Physics **138**, 224705 (2013); doi: 10.1063/1.4809986
View online: http://dx.doi.org/10.1063/1.4809986
View Table of Contents: http://scitation.aip.org/content/aip/journal/jcp/138/22?ver=pdfcov
Published by the AIP Publishing

Impact of doping on the ionic conductivity of ceria: A comprehensive model

Hao Wang,[1] Alexander Chroneos,[2,3] and Udo Schwingenschlögl[1,a)]
[1]*KAUST, PSE Division, Thuwal 23955-6900, Kingdom of Saudi Arabia*
[2]*Department of Materials, Imperial College London, London SW7 2BP, United Kingdom*
[3]*Materials Engineering, The Open University, Milton Keynes MK7 6AA, United Kingdom*

(Received 11 February 2013; accepted 24 May 2013; published online 13 June 2013)

Doped ceria is considered as an electrolyte for solid oxide fuel cell applications. The introduction of dopants in the ceria lattice will affect its electronic structure and, in turn, its ionic conductivity. Simulation of these issues using density functional theory becomes complicated by the random distribution of the constituent atoms. Here we use the generalized gradient approximation with on-site Coulomb interaction in conjunction with the special quasirandom structures method to investigate 18.75% and 25% Y, Gd, Sm, Pr, and La doped ceria. The calculated lattice constants and O migration energies allow us to explain the behavior of the conductivity as obtained in experiments.
 [http://dx.doi.org/10.1063/1.4809986]

I. INTRODUCTION

Research on solid oxide fuel cells and related devices is driven by the requirement for clean, sustainable, and efficient processes for energy conversion.[1–4] To this aim, it is important to lower the operating temperature towards the intermediate temperature range (500 °C–700 °C) where issues such as materials degradation will be ameliorated.[5,6] Presently, there are numerous candidate oxides which are considered for cathode and electrolyte applications for the next generation of intermediate temperature solid oxide fuel cells.[7–12]

In previous studies of reduced CeO_2,[13] charge transport was demonstrated to be achieved by a hopping process of O vacancies and the related distortions. This mechanism is in agreement with the O defect model established by careful measurements of the electrical conductivity of reduced CeO_2 as a function of temperature and O_2 pressure in Ref. 14. In order to improve the ionic conductivity, lower valence cations are doped into CeO_2 to increase the O vacancy concentration. Fluorite-structured solid solutions, such as $Ce_{1-x}M_xO_{2-x/2}$ and $Zr_{1-x}M_xO_{2-x/2}$ (where M is a rare-earth ion), are very good O conducting electrolytes.[15] $Ce_{1-x}M_xO_{2-x/2}$ is particularly important as it has a sufficiently high ionic conductivity and therefore is one of the most promising materials to be integrated in intermediate temperature solid oxide fuel cells.[16] Operation at such temperatures will allow for the integration of low chromium steels, which in turn will reduce cathode degradation from chromium poisoning.[17] Domain boundaries can impact O diffusion in electrolyte materials of solid oxide fuel cells. However, these issues cannot be realistically represented using density functional as they would lead to an enormous computational complexity. Still, it is very fruitful to investigate the O diffusion in single crystals, which can be achieved within density functional theory.

Previous computational studies on $Ce_{1-x}M_xO_{2-x/2}$ have focused on the influence of composition and external parameters (for example, strain) on the O diffusion.[18–22] Andersson and co-workers have investigated the O migration and the vacancy-dopant association for low dopant concentrations.[23] Similar concentrations have been studied by Nakayama and co-workers.[24] The aim of the present work is to understand the impact of dopants on the electronic structure and ionic conductivity for technologically relevant dopant concentrations. We therefore address 18.75% and 25% Y, Gd, Sm, Pr, and La doped ceria, which corresponds to 9% and 12% M_2O_3 doping. The cerium oxide phase diagram[25] suggests that the compound forms ordered lattices at high temperature. For the O vacancy concentrations employed in the present study it still has the fluorite structure.

II. METHODOLOGY

All the calculations are performed by the Vienna *Ab initio* Simulation Package.[26] The exchange correlation is treated in the generalized gradient approximation (Perdew-Burke-Ernzerhof parameterization[27]). The energy cutoff for the plane wave basis set is 400 eV and pseudopotentials generated by the projector augmented wave method[28] are employed. The valence electron configuration is assumed to be $5s^25p^66s^24f^2$ for Ce, $4s^24p^65s^24d^1$ for Y, and $5s^25p^66s^25d^1$ for La. Trivalent Gd, Sm, and Pr pseudopotentials are used, where the 4*f* electrons are treated as core states. In addition, a Γ-centered 2 × 2 × 2 k-mesh is employed.

The on-site Coulomb interaction[29] is taken into account for the Ce 4*f* valence states, but not for the less localized M *d* orbitals. For Ce a *U* parameter of 5–7 eV is commonly used.[30–33] In this study, we therefore choose $U = 5$ eV and $J = 0$ eV.[34] Spin polarized calculations are performed to be consistent with experimental findings[35,36] and experimental lattice constants of 5.413 Å, 5.423 Å, 5.431 Å, 5.422 Å, 5.476 Å, and 5.411 Å are taken from Y,[37] Gd,[38] Sm,[39] Pr,[40] and La[38] doped CeO_2 and pure CeO_2,[25] respectively. All structures are fully optimized until the atomic forces are

a)Email: udo.schwingenschlogl@kaust.edu.sa. Tel.: +966(0)544700080.

TABLE I. Lattice constants (in Å) and angles (in degree) of the optimized structures of $Ce_{26}M_6O_{61}$ and $Ce_{24}M_8O_{60}$.

Compound		Y	Gd	Sm	Pr	La
$Ce_{26}M_6O_{61}$	a	5.545	5.557	5.567	5.590	5.591
	b	5.547	5.557	5.566	5.584	5.581
	c	5.553	5.562	5.570	5.588	5.585
	Angles	89.5 90.0 89.9	89.6 90.0 89.9	89.6 89.9 90.0	89.4 89.7 90.0	89.5 89.5 90.0
$Ce_{24}M_8O_{60}$	a	5.567	5.577	5.585	5.617	5.630
	b	5.537	5.548	5.556	5.587	5.600
	c	5.540	5.551	5.560	5.593	5.608
	Angles	90.5 91.6 89.7	90.3 91.2 89.9	90.2 90.9 90.1	90.3 90.5 90.5	90.3 90.2 90.7

smaller than 0.01 eV/Å. The nudged elastic band method[41,42] is applied to calculate the O migration energies. Five images are generated between the relaxed initial and final images. The total energy differences between the saddle point and the initial/final images are taken as the O migration barriers.

Modeling bulk CeO_2 is straightforward with density functional theory as one only needs to take a unit cell and impose periodic boundary conditions. For systems which display atomic disorder and/or where the introduction of dopants induces the formation of O vacancies the situation is more complicated. However, these issues can be overcome by the special quasirandom structures approach, which makes it possible to adequately mimic the statistics of a random alloy in a small supercell.[43–45] The atomistic nature of the special quasirandom structure approach ensures that the distribution of distinct local environments present in real random alloys is maintained. We note that special quasirandom structures are not the lowest energy structures, but in our case about 0.02 eV per formula unit higher in energy. However, since typical operation temperatures are around 600 °C, special quasirandom structures are appropriate for a correct description of the physics. For $Ce_{26}M_6O_{61}$ and $Ce_{24}M_8O_{60}$, the special quasirandom structures of Ref. 34 are used to simulate M_2O_3 doping levels of 9% and 12%. Both are $2 \times 2 \times 2$ supercells of the basic CeO_2 unit cell. Moreover, the number of O atoms is decided by the charge neutrality requirement.

III. RESULTS AND DISCUSSION

The optimized structure parameters resulting from our calculations are shown in Table I. $Ce_{26}M_6O_{61}$ almost keeps a cubic structure in contrast to $Ce_{24}M_8O_{60}$. The fully relaxed $Ce_{24}M_8O_{60}$ structures show significant structural distortions, which is due to the dopants and O vacancies. In general, the optimized cell size for different dopants reveals a linear relation to the ionic radius of the dopant.[46] Due to the systematic error caused by the generalized gradient approximation, all lattice constants increase by around 2.5%. An exception is $Ce_{26}Pr_6O_{61}$ for which the increase is about 3.5% after the optimization. The average lengths of the M–O bonds are 2.40 Å, 2.42 Å, 2.44 Å, 2.47 Å, and 2.48 Å for Y, Gd, Sm, Pr, and La, respectively.

We find that spin polarized calculations always converge to nonmagnetic solutions. The reason is that the M ions are trivalent so that Ce is the only tetravalent ion in charge neutral $Ce_{26}M_6O_{61}$ and $Ce_{24}M_8O_{60}$. However, this is not an issue for the following considerations, since experimentally the ferromagnetism[35,36] is also very weak. The total density of states (DOS) is addressed in Fig. 1 for different dopants and the two compositions. The electronic states from −3.8 to 0 eV are mainly due to the O 2*p* orbitals, where the M *d* and Ce 4*f* orbitals give very small contributions. The Ce 4*f* states are prominent between −1.5 and 0 eV and the M *d* states in the region from −3.1 to −1.5 eV. The states located between 2 and 3 eV are dominated by the Ce 4*f* orbitals. Moreover, the bandgap is determined by the top of the O 2*p* group of states and the bottom of the empty Ce 4*f* states. We find that the bandgap of $Ce_{24}M_8O_{60}$ is slightly reduced by the fact that Ce 4*f* states expand below 2 eV, as highlighted by the arrow in Fig. 1(b), due to the structural relaxation. The calculated bandgaps are summarized in Table II.

In both compositions, each O atom has four nearest neighbor cations, which are either Ce or dopants. O atoms with four nearest neighbor Ce atoms and three nearest neighbor dopants are denoted as O_{Ce} and O_M, respectively. The partial DOSs of other O atoms show an intermediate state between O_{Ce} and O_M. Partial DOSs of O_M are shown in Fig. 2. We find that the O_M 2*p* orbital contributes more states than the O_{Ce} 2*p* orbital in the energy interval from −0.5 to 0 eV, indicating that the M−O_M bonds are less stable than the Ce−O_{Ce} bonds.

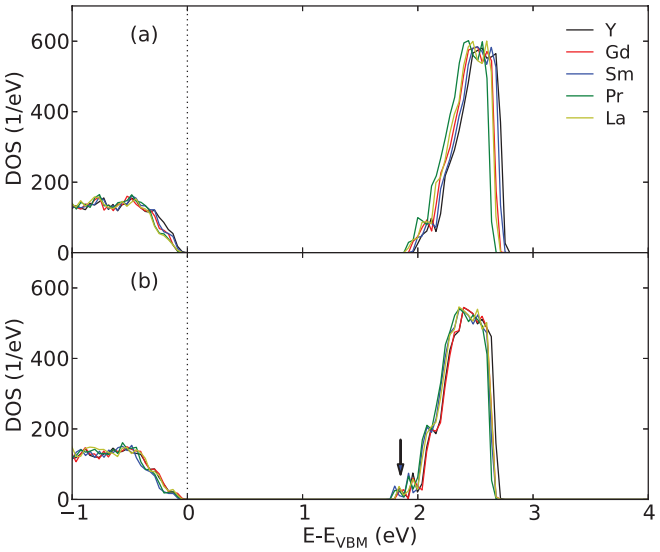

FIG. 1. Total DOS for (a) $Ce_{26}M_6O_{61}$ and (b) $Ce_{24}M_8O_{60}$.

TABLE II. Bandgaps (in eV) of $Ce_{26}M_6O_{61}$ and $Ce_{24}M_8O_{60}$.

	Y	Gd	Sm	Pr	La
$Ce_{26}M_6O_{61}$	1.92	1.87	1.89	1.83	1.85
$Ce_{24}M_8O_{60}$	1.76	1.76	1.70	1.72	1.74

Figure 3 shows the average M *d* DOSs in both compositions. Figures 3(a) and 3(b) are similar except that the former reveals stronger peaks around −2.5 eV, which is due to the fact that $Ce_{26}M_6O_{61}$ is less distorted and disordered than $Ce_{24}Gd_8O_{60}$. The Gd 5*d* DOS is higher than that of La, Pr, and Sm, because Gd has the largest electronegativity.

To investigate the effects on the ionic conductivity for different dopants, the O migration energy in $Ce_{26}M_6O_{61}$ is calculated by the nudged elastic band method. The O diffusion directions are sketched in Fig. 4. PATH 1 corresponds to an O atom with two dopant neighbors which moves to the adjacent vacancy site. PATH 2 is for an O atom which has no dopant nearest neighbor. The total energies of the images along PATH 1 and PATH 2 with respect to the energy of the initial image are plotted in Fig. 5(a). The curves reflect the symmetry with respect to the saddle point. Figure 5(b) addresses the O migration barriers along the paths for different dopants. Forward and backward directions are indicated by (a) and (b) for each path, respectively. According to the values, we conclude that the O migration barrier is influenced by two factors: the ionic radius of the dopant and the M−O bond strengths.

For PATH 1(a), La doping turns out to have the largest barrier of 0.98 eV and Y the smallest of 0.57 eV. On this path the O atom moves over one dopant atom and breaks the bond with the other dopant atom. Therefore, the energy barrier is affected by both factors. Comparing the 5*d* states of Gd, Sm, Pr, and La in Fig. 3(a), we observe that the Gd DOS is enhanced as compared to the other dopants, where the La DOS is the smallest. The DOS indicates that Gd keeps more electrons than the other dopants in the M−O bonds. Considering the electronegativities of the dopants, Gd (1.2) has a stronger tendency to attract electrons than Sm (1.17), Pr (1.13), and La (1.1). Hence, the Gd ionic bonds with O are weaker than for other dopants, where La forms the strongest bonds. The 4*d* orbitals of Y are more localized than the 5*d* orbitals of the other dopants so that they overlap less with the O 2*p* orbitals. Thus, the Y−O bonds are weaker than the bonds involving 5*d* orbitals. On the other hand, La has a larger ionic radius (1.300 Å) than to Pr (1.266 Å), Sm (1.219 Å), and Gd (1.193 Å).[47] This explains the trend which we obtain for the O migration barriers for PATH 1(a), see Fig. 5(b). The slope of

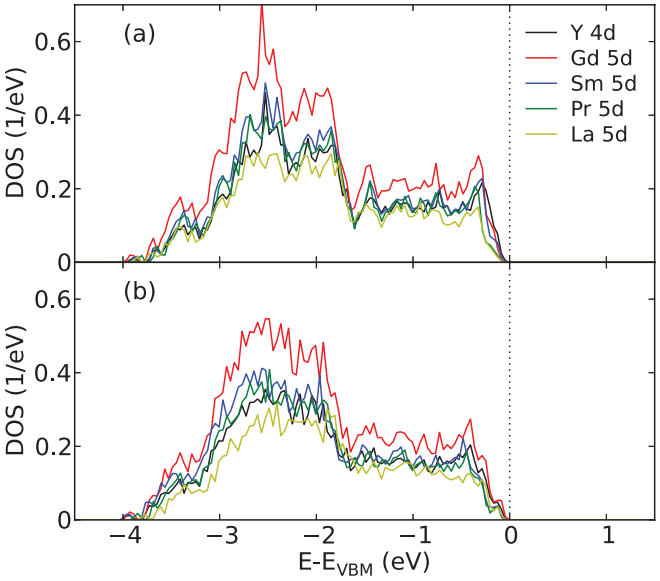

FIG. 3. M *d* DOS for (a) $Ce_{26}M_6O_{61}$ and (b) $Ce_{24}M_8O_{60}$.

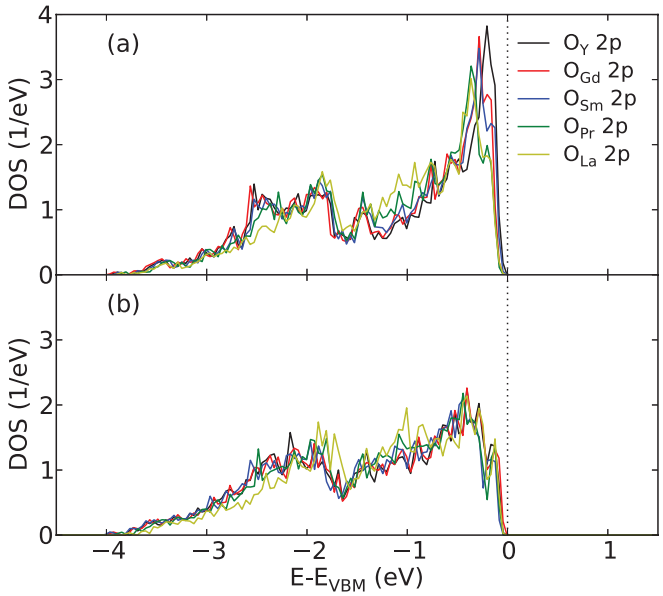

FIG. 2. O 2*p* DOS of atoms with three nearest neighbor dopant atoms in (a) $Ce_{26}M_6O_{61}$ and (b) $Ce_{24}M_8O_{60}$.

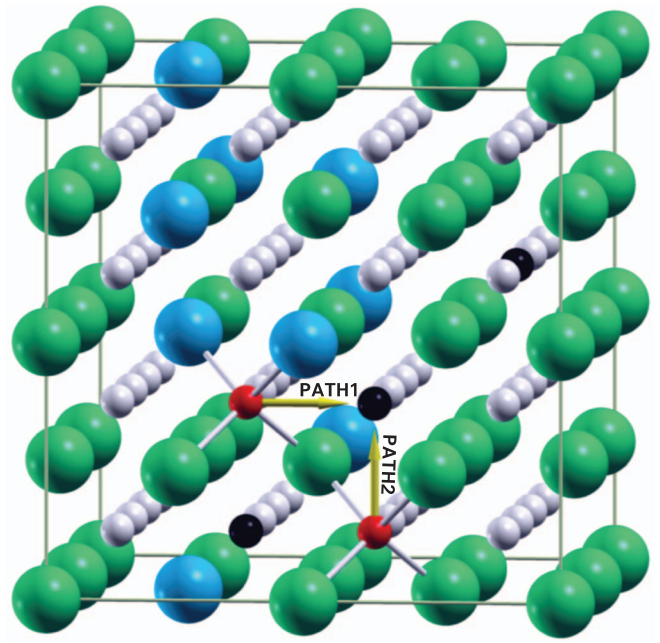

FIG. 4. O migration directions in $Ce_{26}M_6O_{61}$. Green (large light gray) spheres represent the Ce ions, blue (large dark gray) spheres the M ions, red (small) spheres the O ions, and black spheres the O vacancies.

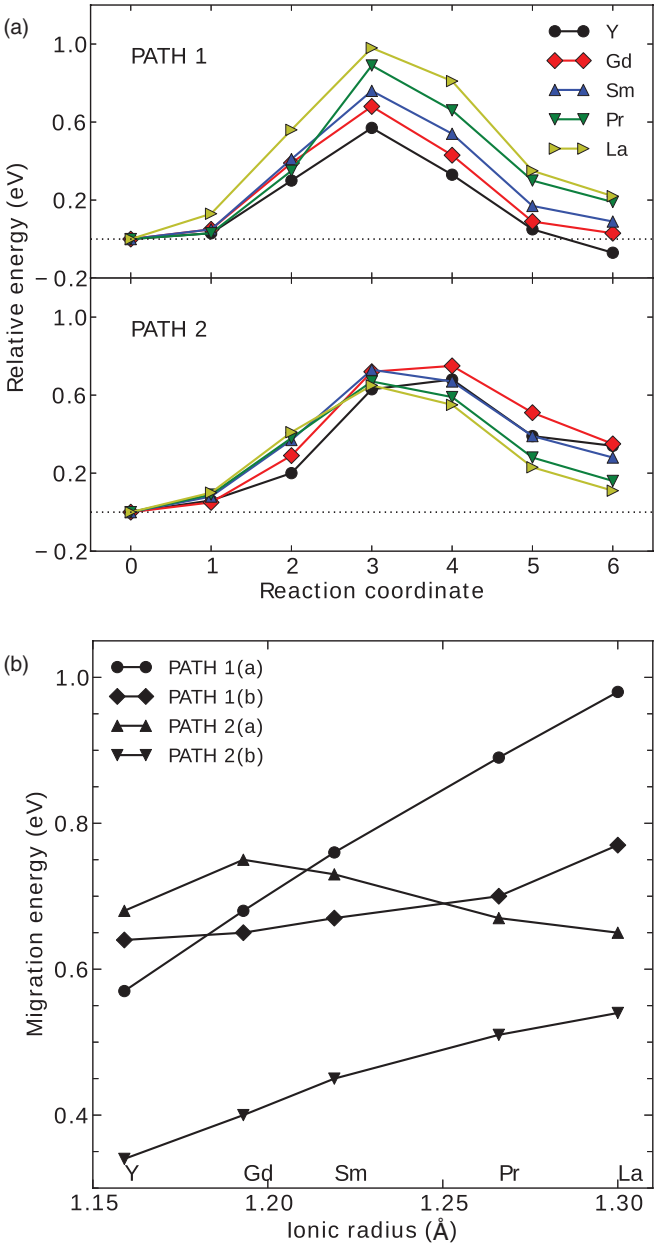

FIG. 5. (a) Total energies relative to the initial images of PATH 1 and PATH 2. (b) Calculated migration energies (in eV) for diffusion forward (a) and backward (b) along PATH 1 and PATH 2 in $Ce_{26}M_6O_{61}$ as a function of the ionic radius of the dopants.

the curve is large because the ionic radius and bond strength act in a cooperative manner.

For PATH 1(b) the migration barriers increase from Y to La because the ionic radius becomes larger. PATH 2(a) goes via Ce and not via a dopant so that the barriers are not affected by the ionic radius directly but rather by the induced structural distortion. On PATH 2(b) the O atom moves over Ce and breaks the bond with the dopant. As a consequence, the calculated values for the energy barrier reflect the strengths of the different M−O bonds, as discussed above.

Experiments for $Ce_{0.2}M_{0.8}O_{2-\delta}$ demonstrate that under the same experimental conditions La doping yields a worse conductivity than Y doping[37] and that Sm doping is less favorable than Gd doping.[39] Gd and Sm doped ceria both show a larger O conductivity than Y doped ceria.[48,49] In Table III this conductivity order is also indicated by the experimental activation energies. Note that only values from the same reference can be safely compared. In addition, our O migration barriers are in reasonable agreement with previous results[23,50–52] based on density functional theory. In general, the conductivity in doped ceria is mainly an ionic conductivity and therefore not only affected by O vacancies but also by the distortion of the crystal lattice.[53] The closer the structure is related to the pure CeO_2 lattice, the better will be the ionic conductivity of the system. The activation energies derived experimentally by the Arrhenius equation include all the factors influencing the conductivity, in particular, the lattice distortion and O migration barriers.

TABLE III. Experimental activation energies and theoretical O migration barriers for doped CeO_2.

Dopant	Experimental (eV)	Theoretical (eV)
Y	0.90,[37] 0.93,[48] 0.77[49]	0.92[50]
Gd	0.90[48]	0.59[51]
Sm	0.69[49]	0.39[23]
Pr	0.76[40]	0.78[52]
La	0.95[37]	0.81[23]

As compared to the optimized lattice constant of 5.552 Å of pure CeO_2, our results show that $Ce_{26}La_6O_{61}$ is subject to a significant lattice distortion as well as a higher O migration barrier than other doping cases. Taking into account the results of Sm and Gd doping, the outcome of our calculations agrees with the experimental finding that La has the worst and Gd the best impact on the conductivity of $Ce_{0.2}M_{0.8}O_{2-\delta}$. No experimental result is reported which would directly compare $Ce_{0.2}Pr_{0.8}O_{2-\delta}$ to other single doping systems. However, we may conclude that $Ce_{0.2}Pr_{0.8}O_{2-\delta}$ is better than La doping and worse than Sm doping for the ionic conductivity, according to the lattice constants and migration energies. Y doping has not been included in the discussion of the 5*d* elements before, because this 4*d* element shows distinct differences in its behavior due to the more localized nature of the electronic states. The experiments indicate that Y doped ceria has a lower conductivity than found for Gd and Sm doping. In our calculation the O migration barrier is lower. However, this is not a contradiction to experiment, because the vacancy-dopant association energy is higher than for the other dopants.

IV. CONCLUSION

Spin polarized *ab initio* calculations have been performed for special quasirandom structures of $Ce_{26}M_6O_{61}$ and $Ce_{24}M_8O_{60}$ to describe M doping levels 18.75% and 25% in CeO_2. The fully optimized structures indicate enhanced distortions for increasing concentrations of dopants and O vacancies. Importantly, these distortions cause the bottom of the empty Ce 4*f* states to appear at lower energy. As a result, the bandgap slightly decreases. Comparing to an O atom without dopant next to it, the O 2*p* orbitals are affected by neighboring dopants to contribute more states around the Fermi energy.

It is revealed that the O migration energy is influenced by the ionic radius of the dopants as well as the M−O bond strength. The conductivity order for different dopants in CeO_2 (except for Y) derived from the calculated lattice constants and O migration barriers agrees with the experiment.

[1] B. C. H. Steele and A. Heinzel, Nature (London) **414**, 345 (2001).
[2] C. Frayret, A. Villesuzanne, and M. Pouchard, Chem. Mater. **17**, 6538 (2005).
[3] M. Yashima, M. Enoki, T. Wakita, R. Ali, Y. Matsushita, F. Izumi, and T. Ishihara, J. Am. Chem. Soc. **130**, 2762 (2008).
[4] Z. Cai, M. Kubicek, J. Fleig, and B. Yildiz, Chem. Mater. **24**, 1116 (2012).
[5] N. P. Brandon, S. Skinner, and B. C. H. Steele, Annu. Rev. Mater. Res. **33**, 183 (2003).
[6] A. J. Jacobson, Chem. Mater. **22**, 660 (2010).
[7] A. Tarancón, S. J. Skinner, R. J. Chater, F. Hernádez-Ramírez, and J. A. Kilner, J. Mater. Chem. **17**, 3175 (2007).
[8] J. Hermet, G. Geneste, and G. Dezanneau, Appl. Phys. Lett. **97**, 174102 (2010).
[9] A. Kushima and B. Yildiz, J. Mater. Chem. **20**, 4809 (2010).
[10] A. Kushima, D. Parfitt, A. Chroneos, B. Yildiz, J. A. Kilner, and R. W. Grimes, Phys. Chem. Chem. Phys. **13**, 2242 (2011).
[11] M. I. Houchati, M. Ceretti, C. Ritter, and W. Paulus, Chem. Mater. **24**, 3811 (2012).
[12] M. Burriel, J. Peña-Martínez, R. J. Chater, S. Fearn, A. V. Berenov, S. J. Skinner, and J. A. Kilner, Chem. Mater. **24**, 613 (2012).
[13] H. L. Tuller and A. S. Nowick, J. Phys. Chem. Solids **38**, 859 (1977).
[14] H. L. Tuller and A. S. Nowick, J. Electrochem. Soc. **126**, 209 (1979).
[15] D. Marrocchelli, P. A. Madden, S. T. Norberg, and S. Hull, Chem. Mater. **23**, 1365 (2011).
[16] M. Burbano, S. T. Norberg, S. Hull, S. G. Eriksson, D. Marrocchelli, P. A. Madden, and G. W. Watson, Chem. Mater. **24**, 222 (2012).
[17] S. P. Jiang and Y. Zhen, Solid State Ionics **179**, 1459 (2008).
[18] H. T. Chen and J. G. Chang, J. Chem. Phys. **132**, 214702 (2010).
[19] P. P. Dholabhai, J. B. Adams, P. A. Crozier, and R. Sharma, J. Mater. Chem. **21**, 18991 (2011).
[20] A. Chroneos, B. Yildiz, A. Tarancón, D. Parfitt, and J. A. Kilner, Energy Environ. Sci. **4**, 2774 (2011).
[21] M. J. D. Rushton, A. Chroneos, S. J. Skinner, J. A. Kilner, and R. W. Grimes, Solid State Ionics **230**, 37 (2013).
[22] M. Nakayama, H. Ohshima, M. Nogami, and M. Martin, Phys. Chem. Chem. Phys. **14**, 6079 (2012).
[23] D. A. Andersson, S. I. Simak, N. V. Skorodumova, I. A. Abrikosov, and B. Johansson, Proc. Natl. Acad. Sci. U.S.A. **103**, 3518 (2006).
[24] M. Nakayama and M. Martin, Phys. Chem. Chem. Phys. **11**, 3241 (2009).
[25] L. Eyring, in *Handbook on the Physics and Chemistry of Rare Earths*, edited by K. A. Gschneider and L. Eyring (North-Holland, Amsterdam, 1979), Vol. 3, Chap. 27.
[26] G. Kresse and D. Joubert, Phys. Rev. B **59**, 1758 (1999).
[27] J. P. Perdew, M. Ernzerhof, and K. Burke, J. Chem. Phys. **105**, 9982 (1996).
[28] P. E. Blöchl, Phys. Rev. B **50**, 17953 (1994).
[29] A. I. Liechtenstein, V. I. Anisimov, and J. Zaanen, Phys. Rev. B **52**, R5467 (1995).
[30] V. I. Anisimov and O. Gunnarsson, Phys. Rev. B **43**, 7570 (1991).
[31] N. C. Hernández, R. Grau-Crespo, N. H. de Leeuw, and J. F. Sanz, Phys. Chem. Chem. Phys. **11**, 5246 (2009).
[32] A. Ismail, J. Hooper, J. B. Giorgi, and T. K. Woo, Phys. Chem. Chem. Phys. **13**, 6116 (2011).
[33] M. Burbano, D. Marrocchelli, B. Yildiz, H. L. Tuller, S. T. Norberg, S. Hull, P. A. Madden, and G. W. Watson, J. Phys.: Condens. Matter **23**, 255402 (2011).
[34] H. Wang, A. Chroneos, C. Jiang, and U. Schwingenschlögl, Phys. Chem. Chem. Phys. **14**, 11737 (2012).
[35] G. R. Li, D. L. Qu, L. Arurault, and Y. X. Tong, J. Phys. Chem. C **113**, 1235 (2009).
[36] R. K. Singhal, P. Kumari, A. Samariya, S. Kumar, S. C. Sharma, Y. T. Xing, and E. B. Saitovitch, Appl. Phys. Lett. **97**, 172503 (2010).
[37] X. Sha, Z. Lü, X. Huang, J. Miao, Z. Ding, X. Xin, and W. Su, J. Alloys Compd. **428**, 59 (2007).
[38] S. Sameshima, H. Ono, K. Higashi, K. Sonoda, Y. Hirata, and Y. Ikuma, J. Ceram. Soc. Jpn. **108**, 1060 (2000).
[39] W. Huang, P. Shuk, and M. Greenblatt, Solid State Ionics **100**, 23 (1997).
[40] P. Shuk and M. Greenblatt, Solid State Ionics **116**, 217 (1999).
[41] G. Mills, H. Jonsson, and G. K. Schenter, Surf. Sci. **324**, 305 (1995).
[42] H. Jonsson, G. Mills, and K. W. Jacobsen, "Nudged elastic band method for finding minimum energy paths of transitions," in *Classical and Quantum Dynamics in Condensed Phase Simulations*, edited by B. J. Berne, G. Ciccotti, and D. F. Coker (World Scientific, 1998).
[43] A. Zunger, S. H. Wei, L. G. Ferreira, and J. E. Bernard, Phys. Rev. Lett. **65**, 353 (1990).
[44] C. Jiang, C. Wolverton, J. Sofo, L. Q. Chen, and Z. K. Liu, Phys. Rev. B **69**, 214202 (2004).
[45] S. T. Murphy, A. Chroneos, C. Jiang, U. Schwingenschlögl, and R. W. Grimes, Phys. Rev. B **82**, 073201 (2010).
[46] S. J. Hong and A. V. Virkar, J. Am. Ceram. Soc. **78**, 433 (1995).
[47] R. D. Shannon, Acta Cryst. A **32**, 751 (1976).
[48] X. Guan, H. Zhou, Z. Liu, Y. Wang, and J. Zhang, Mater. Res. Bull. **43**, 1046 (2008).
[49] X. Sha, Z. Lü, X. Huang, J. Miao, L. Jia, X. Xin, and W. Su, J. Alloys Compd. **424**, 315 (2006).
[50] H. Yoshida, T. Inagaki, K. Miura, M. Inaba, and Z. Ogumi, Solid State Ionics **160**, 109 (2003).
[51] P. P. Dholabhai, J. B. Adams, P. Crozier, and R. Sharma, Phys. Chem. Chem. Phys. **12**, 7904 (2010).
[52] P. P. Dholabhai, J. B. Adams, P. Crozier, and R. Sharma, J. Chem. Phys. **132**, 094104 (2010).
[53] D. J. Kim, J. Am. Ceram. Soc. **72**, 1415 (1989).